

# **Electrocapillary flow in Melcher – Taylor experimental setup**

**Alexander Yu. Gelfgat**

*School of Mechanical Engineering, Faculty of Engineering, Tel-Aviv University, Ramat Aviv,  
Tel-Aviv 6997801, Israel*

**Gerrit Maik Horstmann**

*Helmholtz-Zentrum Dresden - Rossendorf, Bautzner Landstr. 400, 01328 Dresden, Germany*

## Abstract

Electrocapillary two-phase flow in a confined cavity is studied. The flow configuration corresponds to a classical experiment of Melcher and Taylor. It is shown that the computed streamlines of the flow of the heavier liquid (corn oil) qualitatively represents the corresponding experimental image. With the increase of electrocapillary forcing, the flow pattern changes, so that the main circulation localizes near boundary with a larger electric potential. It is shown that numerical results satisfy the Lippmann equation connecting electrically induced surface tension with non-uniform surface electric potential.

## 1. Introduction

Electrocapillary flows appear in two-liquid systems under action of an external electric field tangent to the liquid-liquid interface. An excessive surface charge, which can result either from charge carrying particles or polarization of electrically neutral ones, interacts with the external magnetic field, which creates a Coulomb force that drives the flow. This force is located at the interface and sometimes is interpreted as an electrostatic addition to the surface tension.

Melcher and Taylor [1] observed some earlier works, gave a general description of the phenomena of electrocapillarity, and presented several examples of electrocapillary flows. Later studies considered mainly flows of drops and small particles [2-3], thin films and sheets [4-8], electrocapillary instability of quiescent [9-12] and parallel [14-17] flow two-fluid systems, and electrocapillary flows in bounded cylindrical geometries [18-22]. Part of the studies was focused on deformations of the liquid-liquid interface [4-8,22], while other part considered instabilities of quiescent fluid or simple shear flows under effect of the electrocapillary forces [14-17,21]. Analytical solutions for developed electrocapillary driven flows are given in [1] for an infinite layer and a Stokes flow around a drop. Comparing to an extensive literature on similar thermocapillary flows also driven by the surface force (see [23] and references therein), there is a certain lack of results for developed non-linear electrocapillary flows in finite, experimentally realizable, geometry.

In this paper, we address numerically configuration of the simple experiment of [1] that illustrated the electrocapillary driving effect in a rectangular cavity. We show that a two-dimensional numerical model qualitatively represents the experimental observations. We examine how the flow pattern would change with increase of the applied voltage. In addition, we show that our solution obeys the Lippmann equation [24], which describes dependence of the surface tension on the applied voltage.

## 2. Surface force induced by electrocapillarity

Since electrocapillary flows are much less known compared to thermocapillary or concentration-capillary flows, we give a brief introduction to the basic physical principles. The field of Electrohydrodynamics treats flows induced by electric fields in weakly-conducting liquids such as leaky dielectrics or aqueous electrolytes [24-26]. The electromechanical coupling at the interfaces, where electrical parameters are subject to discontinuities, induce unneglectable surface forces that must be accounted for in fluid dynamics models. The effect of electrocapillarity relates to variation of surface tension  $\gamma$  with the local interfacial electrical potential  $V$ , similarly to better known variations of the surface tension with temperature  $T$  or concentration  $c$ . The dependence  $\gamma(T, c)$  is a material property, and usually

is assumed to be linear for the temperature, as well for the concentration. For example, in most liquids  $\partial\gamma/\partial T < 0$ , which defines direction of the thermocapillary force from warmer to colder interface regions. In the electrocapillary flows dependence of the surface tension on the local electric voltage  $V$  is not monotonic, usually parabolic  $\gamma \sim V^2$ , so that the sign of  $\partial\gamma/\partial V$  can change. The parabolic dependence follows from the Lippmann equation [27,28], which, under the constraint that liquid composition and temperature remain quasi-constant, states

$$\frac{\partial\gamma}{\partial V} = -q_s \quad , \quad (1)$$

where  $q_s$  is the interface electric charge. The latter can be either induced by external electric fields, or result from covalently bound ionizable groups, or ion adsorption in electrochemical systems [26,29]. However, the charge density is not a material constant, but results from electrohydrodynamics of the whole system. To avoid consideration of the full electrohydrodynamic problem, the interface can be assigned with a specific capacitance  $C$ , such that  $q_s = C(V - V_0)$ , where  $V_0$  denotes the potential of zero charge, which is nonzero in most electrochemical systems. In the particular case of the dielectric Melcher & Taylor (1969) experiment addressed in this paper, an external potential difference is needed to induce surface charges, and the capacitance is simply given by the electric permittivity and the normal distance between the electrodes,  $C = \varepsilon_0/a$  (see below). Substituting  $q_s = C(V - V_0)$  into equation (1) and integrating yields the parabolic electrocapillary profile

$$\gamma = \gamma_0 - \frac{1}{2}C(V - V_0)^2, \quad (2)$$

with  $\gamma_0 = \gamma(V = V_0)$  being the surface tension in the discharged case. Equation (1) shows that any increase in charge density, positive or negative, will result in a decrease in the surface tension. This behavior can be intuitively explained by the fact that all interfacial charges exert repulsive Coulomb forces on each other, which are tangential to the interface. A hypothetical expansion of the interface therefore requires less energy resulting in lower surface tension. Electrocapillary flows necessarily develop whenever there is an unbalanced tangential gradient of the surface tension created by tangential voltage gradient, which, in its turn, results from a nonzero tangential electric field component. Contrarily to thermocapillary flows the derivative  $\partial\gamma/\partial V$  changes with polarization ( $V < V_0$  or  $V > V_0$ ), which makes electrocapillary forcing more complicated, potentially exhibiting both destabilizing or stabilizing effect. Apparently, to attain sufficiently large tangential stresses that can noticeably affect macroscopic flows, either the capacitance or the voltage must be large enough. In dielectrics, the capacitance is very small such that voltages in the order of kilovolts must be applied to drive considerable flows. In contrast, the capacitance of electrochemical double layers is very high, allowing to reach similar tangential stresses only with a few volts. As a last point, it should be mentioned that the introduced electrocapillary effect can also be described and

understood in a fully equivalent way by considering electric Maxwell stresses acting at the interface, see [24,25] for more details.

### 3. Description of a problem

We consider a 2D configuration of the experiment described in Melcher & Taylor [1], see their Figs. 1 and 2. The problem is sketched again in Fig. 1 below. The liquid (corn oil) occupies a rectangular volume of length  $l$  and height  $b$ . The vertical boundaries are electrodes that are at the electric potential difference  $V_0$ . The third electrode is a straight plate, whose left end is attached to the top of the left vertical boundary, and the right end is positioned at the distance  $a$  above the top of the right boundary. Its electric potential is the same as that of the left boundary. The bottom and part of the vertical boundary that connects the second and the third electrodes are assumed to be electrically insulated. The triangular part above the corn oil is filled by air.

Jump of the electrical field vertical component creates an excessive surface charge, whose interaction with the electric field results in the Coulomb force, as explained above and in [1]. We assume that the gravity force is large enough to keep the interface flat, which is consistent with the experimental photo in Fig. 2 of [1]. The horizontal component of the Coulomb force acts along the interface and drives the flow. The whole system represents a two-phase (corn oil – air) flow driven by the tangential Coulomb force acting along the interface.

### 5. Governing equations

We use the leaky dielectric model introduced in [1] and thoroughly re-derived by Saville [24]. Since the electric field is irrotational, it is represented by the gradient of the electric potential  $\mathbf{E} = -\nabla\phi$ . Neglecting the volume electric charges, in each of the phases 1 and 2,

$$\text{div}(\sigma_j \mathbf{E}_j) = -\Delta\phi_j = 0, \quad j = 1, 2. \quad (3)$$

The boundary conditions for the electric potential follow from the description of Fig. 1:

$$\phi_1(x = 0, y) = \phi_2\left(x, y = b + a\frac{x}{l}\right) = 0, \quad (3.1)$$

$$\phi_1(x = l, 0 \leq y \leq b) = V_0, \quad (3.2)$$

$$\frac{\partial\phi_1}{\partial y}(x, y = 0) = \frac{\partial\phi_2}{\partial x}(x = l, b < y \leq b + a) = 0. \quad (3.3)$$

At the interface  $y = b$ :

$$\phi_1(x, y = b) = \phi_2(x, y = b), \quad (4.1)$$

$$\varepsilon_0 [\varepsilon_2 E_{2,y} - \varepsilon_1 E_{1,y}]_{y=b} = \varepsilon_0 \left[ \left( \varepsilon_1 \frac{\partial \phi_1}{\partial y} - \varepsilon_2 \frac{\partial \phi_2}{\partial y} \right) \right]_{y=b} = q_s, \quad (4.2)$$

where  $q_s$  is the surface charge. To close formulation for the electric field, we need to add equation describing conservation of the surface charge, which will include the flow velocity and will be discussed later.

The flow is described by the momentum and continuity equations in each phase

$$\rho_j \left[ \frac{\partial \mathbf{u}_j}{\partial t} + (\mathbf{u}_j \cdot \nabla) \mathbf{u}_j \right] = -\nabla p_j + \mu_j \Delta \mathbf{u}_j, \quad (5)$$

$$\nabla \cdot \mathbf{u}_j = 0, \quad (6)$$

with no-slip boundary conditions at all the boundaries

$$\mathbf{u}_j(x, y = 0) = \mathbf{u}_j(x = 0, y) = \mathbf{u}_j(x = l, y) = \mathbf{u}_j(x, y = b + a \frac{x}{l}) = 0. \quad (7)$$

Here  $t$  is time,  $\rho_j$  and  $\mu_j$  are density and viscosity of the fluids. For the flat interface, the normal to interface velocity is zero,

$$u_y(x, y = b) = 0. \quad (8)$$

The tangent stress balance at the interface reads

$$\left[ \mu_2 \frac{\partial u_{2,x}}{\partial y} - \mu_1 \frac{\partial u_{1,x}}{\partial y} \right]_{y=b} = q_s E_x(x, y = b) = q_s \left[ \frac{\partial \phi}{\partial x} \right]_{y=b}. \quad (9)$$

In the work of Saville [24] the conservation of surface charge is described by equation (22'), in which the charge diffusion is neglected. Also, the origin of the velocity dependent terms is not completely clear. In our opinion, keeping the diffusion term is essential, since otherwise it will be impossible to arrive to a steady distribution of the surface charge in a quiescent fluid. In the following we use the equation derived in [29] and used in [15], which reads for an arbitrary interface

$$\frac{\partial q_s}{\partial t} + u_n (\nabla \cdot \mathbf{n}) q_s + \nabla_s \cdot \mathbf{K}_s + \mathbf{n} \cdot \llbracket \sigma \mathbf{E} \rrbracket - u_n \llbracket q \rrbracket = 0, \quad (10)$$

where

$$\mathbf{K}_s = \xi_s q_s \mathbf{E}_s + \sigma_s \mathbf{E}_s + q_s \mathbf{u}_s - D_s \nabla q_s. \quad (11)$$

Here  $\mathbf{n}$  is the normal to the interface,  $\xi_s$  is the surface electrical mobility of ions,  $\sigma_s$  is interface electrical conductivity,  $D_s$  is the surface diffusion coefficient,  $u_n$  is the normal to the surface velocity, and  $(\nabla \cdot \mathbf{n})$  represents the interface curvature. The operator  $\nabla_s$  is the projection of the operator  $\nabla$  on the interface and is defined as  $\nabla_s = \nabla - \mathbf{n}(\mathbf{n} \cdot \nabla)$ . The double square brackets denote jump of a quantity from phase 1 to phase 2. A similar formulation can be found in [26].

For the present problem  $u_n = 0$ ,  $(\nabla \cdot \mathbf{n}) = 0$ , and  $\nabla_s = \partial/\partial x$ . Therefore, for a steady flow, Eqs. (9) and (10) yield

$$\xi_s \frac{\partial}{\partial x} (q_s E_x) + \sigma_s \frac{\partial E_x}{\partial x} + q_s u_x - D_s \frac{\partial^2 q_s}{\partial x^2} + (\sigma_1 E_{1,y} - \sigma_2 E_{2,y}) = 0 . \quad (12)$$

Considering boundary conditions for the surface charge, we assume that there is no flux of the surface charge through the left boundary. For the right boundary this assumption leads to a discontinuity in the derivative  $\frac{\partial q_s}{\partial y}$  at  $y = b$ . Thus, we derive the boundary condition from Eq. (4.2) taking into account that this boundary is equipotential for  $y \leq b$ . Thus, the boundary conditions are

$$\left[ \frac{\partial q}{\partial x} \right]_{y=b, x=0} = 0, \quad q_s(x=l) = \varepsilon_0 \varepsilon_2 \left[ \frac{\partial \phi_2}{\partial y} \right]_{y=b, x=l}, \quad (13)$$

This closes the set of equation for the considered problem.

The problem is solved using the finite volume discretization on a regular uniform grid. The upper boundary is accounted for by the immersed boundary method. The steady flows are calculated by the Newton method using the approach of [30]. The calculations are performed on 200×200 grid. The convergence study shows that this grid yields three decimal places converged for all computed functions.

## 6. Plane-parallel solution of Melcher and Taylor.

Melcher & Taylor [1] considered the current problem assuming very large length  $l$  and vacuum as the second phase. The electric potential was assumed to be a linear function of  $x$  and  $y$ , so that the horizontal and vertical components of the electric field were constant:

$$\phi = V_0 \left( \frac{x}{l} - \frac{y}{a} \right), \quad E_x = -\frac{\partial \phi}{\partial x} = -\frac{V_0}{l}, \quad E_y = -\frac{\partial \phi}{\partial y} = \frac{V_0}{a}. \quad (14)$$

This yields for the electric charge and the Coulomb tangent stress

$$q_s = \frac{\varepsilon_0 V_0}{a}, \quad \tau_C = -\varepsilon_0 \frac{V_0^2}{al}. \quad (15)$$

Now assuming that owing to a large  $l$ , velocity has only horizontal non-zero component that depends only on the coordinate  $y$ , the problem for velocity becomes

$$\mu \frac{d^2 u_x}{dy^2} = -\frac{dp}{dx}, \quad u_x(y=0) = 0, \quad \mu \left[ \frac{du_x}{dy} \right]_{y=b} = -\varepsilon_0 \frac{V_0^2}{al} \quad (16)$$

The pressure gradient  $\frac{dp}{dx}$  is assumed to be a constant, and is obtained from the requirement of the zero mass flux across the liquid layer

$$\int_0^b u_x dy = 0 \quad (17)$$

The solution of (16), (17) is

$$u_x = -\frac{\varepsilon_0}{2\mu} \frac{V_0^2}{al} \left( \frac{3}{2} \frac{y^2}{b^2} - \frac{y}{b} \right) \quad (18)$$

This is the same parabolic return flow, as the profile of Birikh [31] for thermocapillary convection in a horizontal layer with a horizontal temperature gradient.

## 7. Flow in a finite geometry

For calculations in the finite geometry we use properties of the corn oil listed in Table 1. The values of surface conductivity, mobility, and diffusion coefficient are unknown, and we estimate them by the order of magnitudes of these values published for other materials.

First, we perform calculations considering the finite geometry, but a constant interface Coulomb tension given by Eq. (14). The resulting streamlines are plotted in Fig. 2a. Then, we perform computations for the full model (3)-(13), which results in the streamlines plotted in Fig. 2b. We observe that the flows are similar, and the minimal and maximal values of the stream function are close. The flow along the interface is directed from the right to the left boundary, i.e., from the larger to lower voltage. The maximum of stream function is shifted towards the left boundary, which is consistent with the experimental photo in Fig. 2 of [1]. This is similar to the patterns developing in long horizontal cavities under action of thermocapillary force [32]. Note, that the interface stress drives also the air flow in the upper triangular part of the setup. Owing to the small viscosity of air, its influence on the flow inside the oil is negligible. However, its effect can be more significant if, say, the two liquids are non-isothermal and continuity of heat flux at the interface is required.

Similarities and differences in the description of electric part in the two cases are illustrated in Fig. 3. Figure 3a shows equipotential lines for the full leaky dielectric model. We see that the potential inside the oil is a linear function of  $x$ , and inside the air it is almost linear function of  $x$  and  $y$ , as was assumed by Melcher & Taylor [1]. The difference is clearly seen at the profile of

surface charge (Fig. 3b). The surface charge is almost constant, except a short region near the right boundary, where it steeply grows. The value of constant is  $\approx 6.4 \cdot 10^{-6} \text{ C/m}^2$ , while Eq. (15) yields a close value  $q_s \approx 6.2 \cdot 10^{-6} \text{ C/m}^2$ . The steep growth near the right boundary is caused mainly by the growth of  $\partial\phi/\partial y$  taken at the interface from the air side.

To look for possible flow changes, we varied the last three parameters of Table 1, which are unknown for the corn oil – air system. Increase of the electric mobility to the value of  $10^{-3} \frac{\text{m}^2}{\text{V}\cdot\text{s}}$ , or surface diffusion coefficient to  $0.01 \frac{\text{m}^2}{\text{s}}$ , or surface conductivity to  $10^{-5} 1/\Omega \cdot \text{m}^2$ , did not noticeably alter the whole numerical solution. This shows that added phenomena of surface charges mobility, surface diffusion, and surface conductivity are negligible compared to the effect of the surface charge accumulation owing to the electric field inhomogeneity. It points also on the consistency of the Melcher-Taylor model. At the same time, these meanwhile negligible effects may affect stability of the interface, which yet to be studied.

A possible change takes place with further increase of the interface of the applied voltage. This is illustrated in Fig. 4. We observe that with the increase of voltage, meaning increase of the forcing, the main circulation is shifted towards the left boundary, where the most intensive flow is localized. Again, this is similar to changes of flow patterns of thermocapillary convection with the increase of the Marangoni number [30,32].

Finally, we verify additionally the electrostatic part of our numerical model. The additional surface tension induced by the Coulomb forces is characterized by the surface tension coefficient  $\gamma$ , which is analogous to the mechanical surface tension coefficient, as is discussed in Section 2. The coefficient  $\gamma$  is connected with the local interface voltage by the Lippmann equation (1), which results from thermodynamic relations [28]. These relations are not straightforwardly included in the above mathematical model. Therefore, an examination whether the present results, obtained from the full electrohydrodynamical model, satisfy the Lippmann equation (1), would yield an independent verification. We rewrite r.h.s. of Eq. (9) as

$$q_s E_x(x, y = b) = \frac{\partial \gamma}{\partial x} \quad (18)$$

from which

$$\gamma(x) = \int_0^x q_s E_x(x, y = b) dx \quad . \quad (19)$$



We use the numerical solution to calculate  $\gamma(x)$  and then  $\frac{\partial \gamma}{\partial V} = \frac{\partial \gamma}{\partial \phi}$ , which we compare with calculated profile of  $q_s$ .

The result of this comparison is shown in Fig. 5 for three values of the applied voltage. We observe coincidence of all profiles to within the plot accuracy. We also observe that both compared values are scaled by the applied voltage  $V_0$ . This shows, in particular, that non-linear coupling of the surface charge with velocity in Eq. (12) is weak. Since the velocity and the surface charge are coupled by equations (9) and (12), and the Lippmann equation results from thermodynamic relations, this comparison yields a good verification of the numerical results.

## 8. Concluding remarks

A confined experimental model used by Melcher and Taylor [1] for experimental demonstration of the electrocapillary flow was studied numerically. A qualitative agreement between the calculated streamlines and the experiment flow visualization was obtained. Change of velocity pattern with the increase of the externally applied voltage was examined. It was shown that a stronger forcing leads to the intensification of flow near the boundary having lower electric potential.

An analogy between the electrocapillary and thermocapillary flows is well-known [14]. Also in this study we observe similarity of flows driven by these two different interface forcing mechanisms and give relevant references to the thermocapillary flows results, which had been studied much more intensively than the electrocapillary ones. It can be interesting to examine stability of this flow and to compare it with the stability of its thermocapillary analog [23,30,33]. Another question, yet to be answered, is a possible interfacial instability induced by the electrocapillary effect. However, these tasks are beyond the scope of the present short notice.

Finally, we examine whether our numerical results satisfy the Lippmann equation, which is not a part of our model and is derived from the thermodynamic relations [28]. A good agreement obtained (Fig. 5) verifies the present calculations.

Table 1. Dimensional parameters used in the calculations

Property	Notation	Value
Length, $m$	$k$	0.24
Oil layer height, $m$	$b$	0.038
Air layer height, $m$	$a$	0.028
Corn oil density, $kg/m^3$	$\rho_1$	918.5
Corn oil viscosity, $kg/m \cdot s$	$\mu_1$	0.055
Corn oil electric permittivity	$\varepsilon_1$	3.1
Corn oil electric conductivity, $1/\Omega \cdot m$	$\sigma_1$	$4.58 \cdot 10^{-5}$
Air oil density, $kg/m^3$	$\rho_2$	1.0
Air oil viscosity, $kg/m \cdot s$	$\mu_2$	$1.8 \cdot 10^{-5}$
Air oil electric permittivity	$\varepsilon_2$	$10^{-12}$
Air oil electric conductivity, $1/\Omega \cdot m$	$\sigma_2$	$4.58 \cdot 10^{-5}$
Interface electric conductivity*, $1/\Omega \cdot m^2$	$\sigma_s$	$10^{-10}$
Interface diffusion coefficient*, $m^2/s$	$D_s$	$10^{-09}$
Interface electric mobility of ions*, $m^2/V \cdot s$	$\xi_s$	$10^{-09}$

\* the correct value is unknown

## References

1. Melcher, J. R., Taylor, G. I.: Electrodynamics: A review of the role of interfacial shear stresses, *Ann. Rev. Fluid Mech.* **1**, 111-146 (1969)
2. Gelfgat, A.Y. Tanasawa, I.: Numerical investigation of the thermocapillary drift of a bubble in an electric field, *Microgravity Science and Technology* **8**, 16-22 (1995).
3. Xue, R., Liu, W., Jiang, T., Song, C., Jiang, H., Ren, T.: Pumping of ionic liquids by liquid metal-enabled electrocapillary flow under DC-biased AC forcing, *Adv. Mater. Interfaces* **7**, 2000345 (2020).
4. Georgiou, E., Papageorgiou, D.T., Maldarelli, C., Rumschitki, D.S.: The double layer – capillary stability of an annular electrolyte film surrounding a dielectric – fluid core in a tube, *J. Fluid Mech.* **226**, 149-174 (1991).
5. Tilley, B.S., Petropoulos, P.G., Papageorgiou, D.T.: Dynamics and rupture of planar electrified liquid sheets, *Phys. Fluids* **13**, 3547-3563 (2001).
6. Pease III, L.F., Russel, W. B.: Linear stability analysis of thin leaky dielectric films subjected to electric fields, *J. Non-Newtonian Fluid Mech.* **102**, 233-250 (2002).
7. Papageorgiou, D.T., Vanden-Broeck, J.-M.: Large-amplitude capillary waves in electrified fluid sheets, *J. Fluid Mech.* **508**, 71-88 (2004).
8. Ozen, O., Papageorgiou, D.T., Petropoulos, P.G.: Nonlinear stability of a charged electrified liquid sheet under the action of a horizontal electric field, *Phys. Fluids* **18**, 042102 (2006).
9. Melcher, J. R., Schwarz, W. J., Interfacial relaxation overstability in a tangential electric field, *Phys. Fluids* **11**, 2604-2616 (1968)
10. Aogaki, R., Kitazawa, K., Fueki, K., Mukaibo, T.: Theory of polarographic maximum current – I. Conditions for the onset of hydrodynamic instability in a liquid metal electrode system, *Electrochimica Acta* **23**, 867-874 (1978)
11. Aogaki, R., Kitazawa, K., Fueki, K., Mukaibo, T.: Theory of polarographic maximum current – II. Growth or decay rate of the electrochemical and hydrodynamic instability, *Electrochimica Acta*, **23**, 875-880 (1978)
12. Makino, T., Morioka, K., Aogaki, R.: Occurrence of cellular convective flow accompanying the polarographic maximum wave of the first kind, *J. Electroanal. Chemistry* **190**, 261-265 (1985).
13. Makino, T., Aogaki, R.: Occurrence of regular convection at the liquid-liquid interface of two immiscible electrolyte solutions by resonance with a pulsed potential, *J. Electroanal. Chemistry* **198**, 209-212 (1986).
14. Hu, K.-X., Zheng, S., Zhao, C.-Z., Chen, Q.-S.: Linear stability of electrocapillary convection in an infinite liquid layer, *J. Electrostatics*, **114**, 103619, (2021).
15. Castellanos, A., Gonzales, A.: Nonlinear electrohydrodynamics of free surfaces, *IEEE Transactions on Dielectrics and Electrical Insulation* **5**, 334-343 (1998).
16. Thaokar, R.M. Kumaran, V.: Electrohydrodynamic instability of the interface between two fluids confined in a channel, *Phys. Fluids*, **17**, 084104 (2005).
17. Mählmann, S., Papageorgiou, D.T.: Interfacial instability in electric plane Couette flow, *J. Fluid Mech.* **666**, 155-188 (2011).
18. González, H.: Influence of bounded geometry on electrocapillary instability, *Phys. Rev. B* **50**, 2520-2532 (1994).
19. Uguz, A.K., Ozen, O., Aubry, N.: Electric field effect on a two-fluid interface instability in channel flow for fast electric times, *Phys. Fluids* **20**, 031702 (2008).

20. Burcham, C.L., Saville, D. A.: Electrohydrodynamic stability: Taylor-Melcher theory for a liquid bridge suspended in a dielectric gas, *J. Fluid Mech.* **452**, 163-187 (2002).
21. Herrada, M.A., Barrero, A.: Self-rotation in electrocapillary flows, *Phys. Rev. E* **66**, 036311 (2002).
22. Petrin, A.B.: Electrocapillary instability of a conducting liquid cylinder, *J. Exp. Theor. Phys.* **106**, 963-973 (2008).
23. M. Lappa: *Thermal convection, Patterns, Evolution and Stability*, Wiley & Sons, Singapore (2009)
24. Saville, D. A.: Electrodynamics: The Taylor-Melcher Leaky Dielectric model, *Ann. Rev. Fluid Mech.*, **29**, 27-64 (1997).
25. Johnson, D.: Electrocapillary Flows, In *Interfacial Fluid Dynamics and Transport Processes* (ed. Narayanan, R. & Schwabe, D.), pp. 291–304, Springer, Berlin, Heidelberg, 2003
26. Zhakin, A.I.: Electrohydrodynamics, *Physics – Uspekhi* **55**, 465-488 (2012),
27. Lippmann, G.: Relations entre les phénomènes électriques et capillaires, *Ann Chim Phys* **5**, 494–549 (1875).
28. Bockris, J. O'M., Khan, S.U.M.: *Surface electrochemistry*, Springer, NY, 1993.
29. Castellanos, A.: Basic Concepts and Equations in Electrohydrodynamics, in: *Electrohydrodynamics* (ed. A. Castellanos), Springer, NY, 1998, pp. 1-82.
30. Gelfgat, A. Yu: Stability of convective flows in cavities: solution of benchmark problems by a low-order finite volume method, *Int. J. Numer. Meths. Fluids* **53**, 485-506 (2007).
31. Birikh, R. V.: Thermocapillary convection in a horizontal layer of liquid, *J. Appl. Mech. Tech. Phys.* **3**, 69-72 (1966).
32. Ben Hadid, H., Roux, B.: Thermocapillary convection in long horizontal layers of low-Prandtl-number melts subject to a horizontal temperature gradient, *J. Fluid Mech.* **221**, 77-103 (1990).
33. Gelfgat, A Yu.: Effect of interface dynamic deformations on instabilities of buoyancy-thermocapillary convection in a two-fluid two-layer system, *Physical Review Fluids* **7**, 053503 (2022).

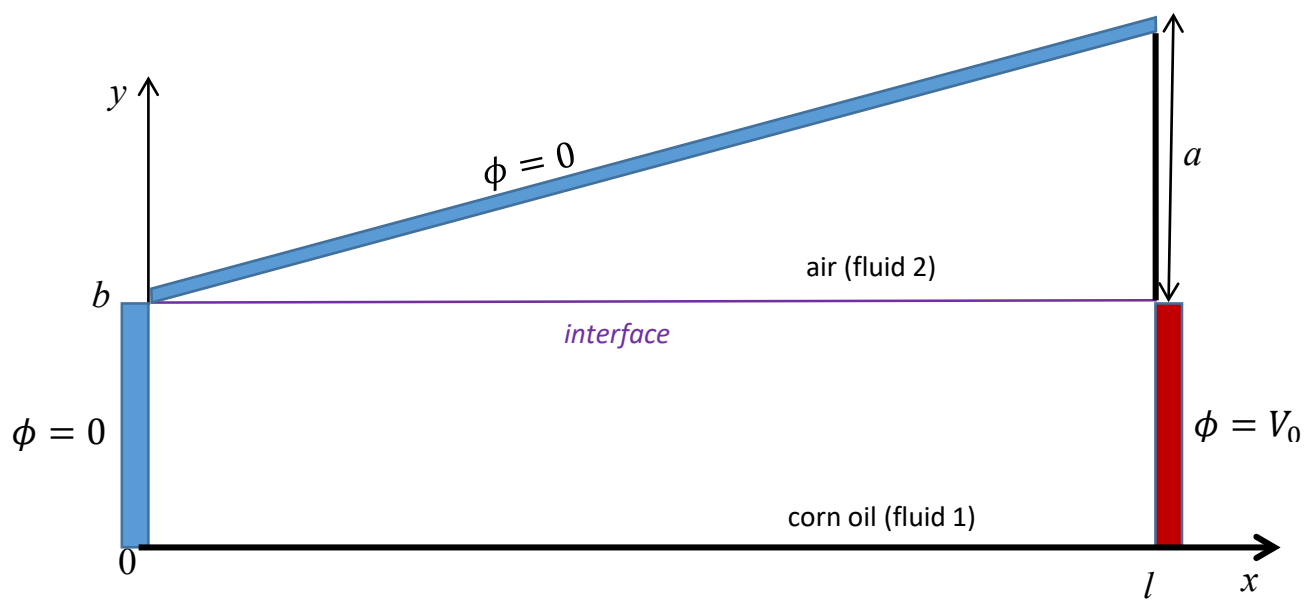


Fig. 1. Sketch of the problem

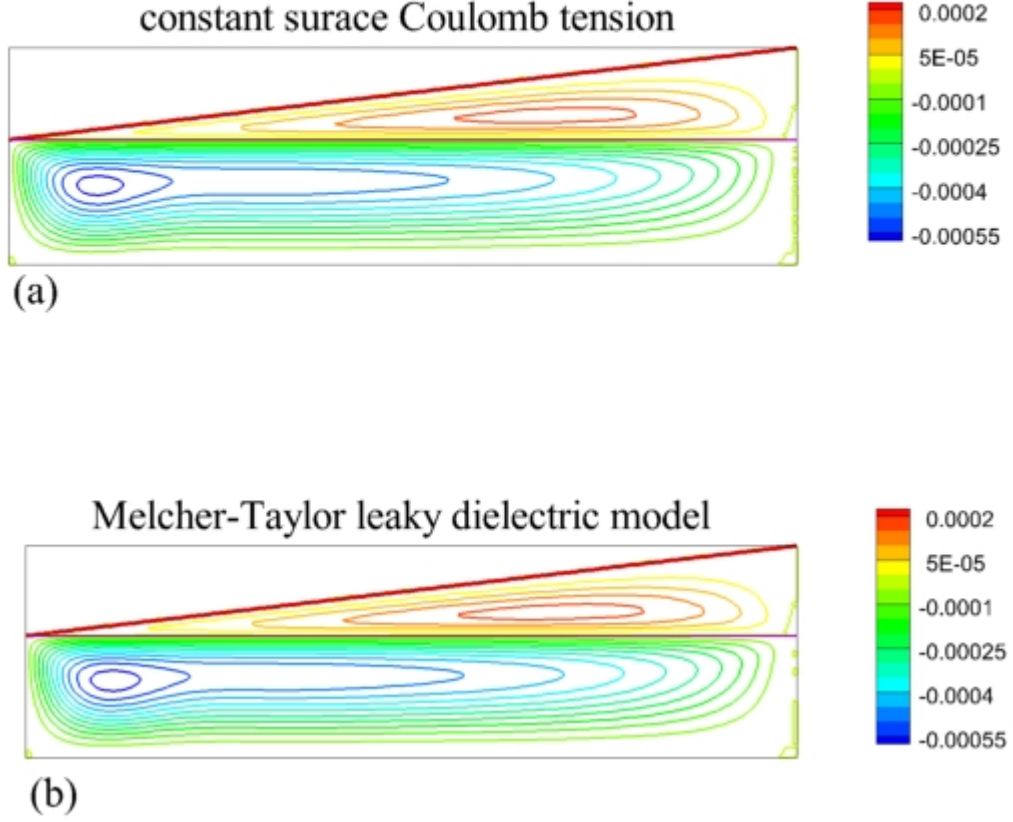


Fig. 2. Flow streamlines for parameters of the experiment [1] at  $V_0 = 20 \text{ kV}$ . (a) with a constant surface Coulomb tension (13);  $\psi_{min} = -0.000569 \text{ m}^2/\text{s}$ ,  $\psi_{max} = 0.000221 \text{ m}^2/\text{s}$ . (b) with a complete leaky dielectric model (1)-(11);  $\psi_{min} = -0.000573 \text{ m}^2/\text{s}$ ,  $\psi_{max} = 0.000222 \text{ m}^2/\text{s}$ . Along the interface the flow is directed for the right to the left boundary.

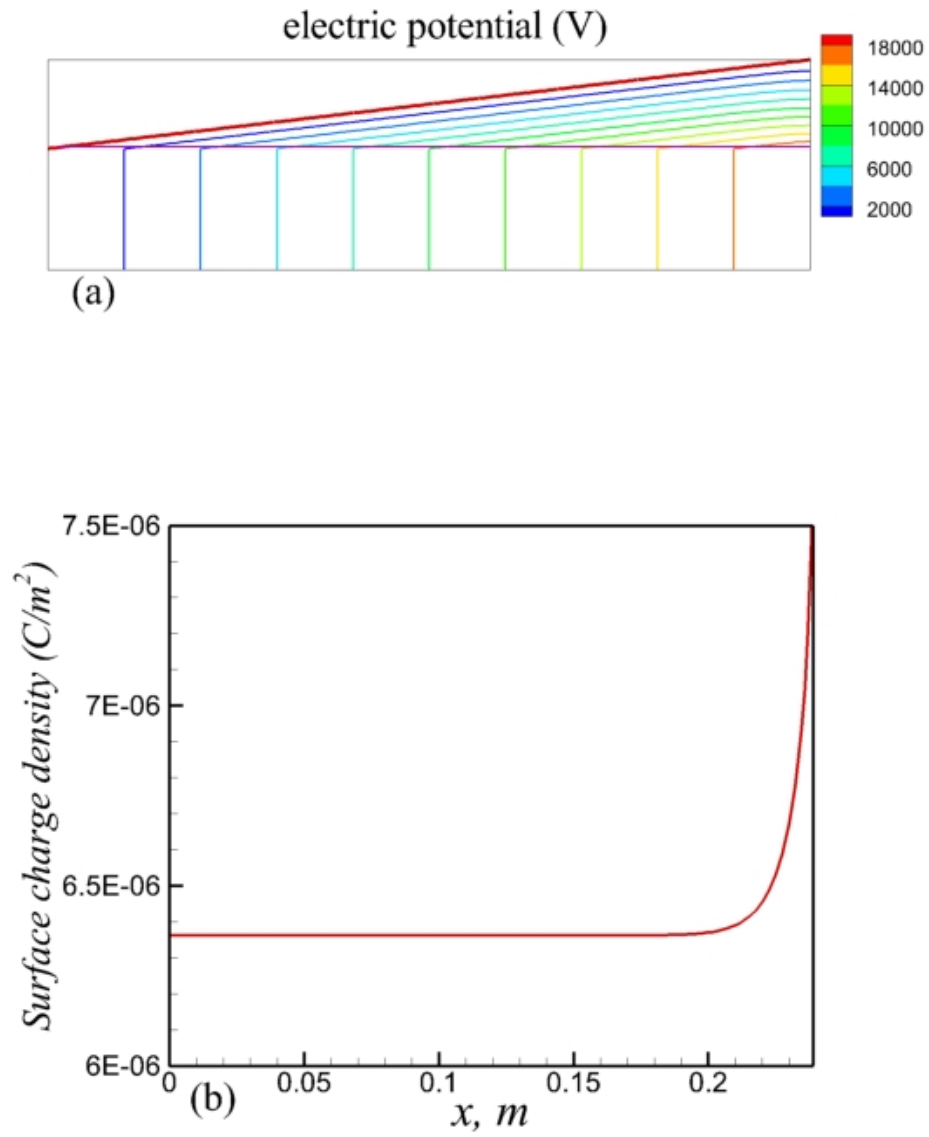


Fig. 3. Equipotential lines (a) and distribution of the surface charge density along the surface (b).

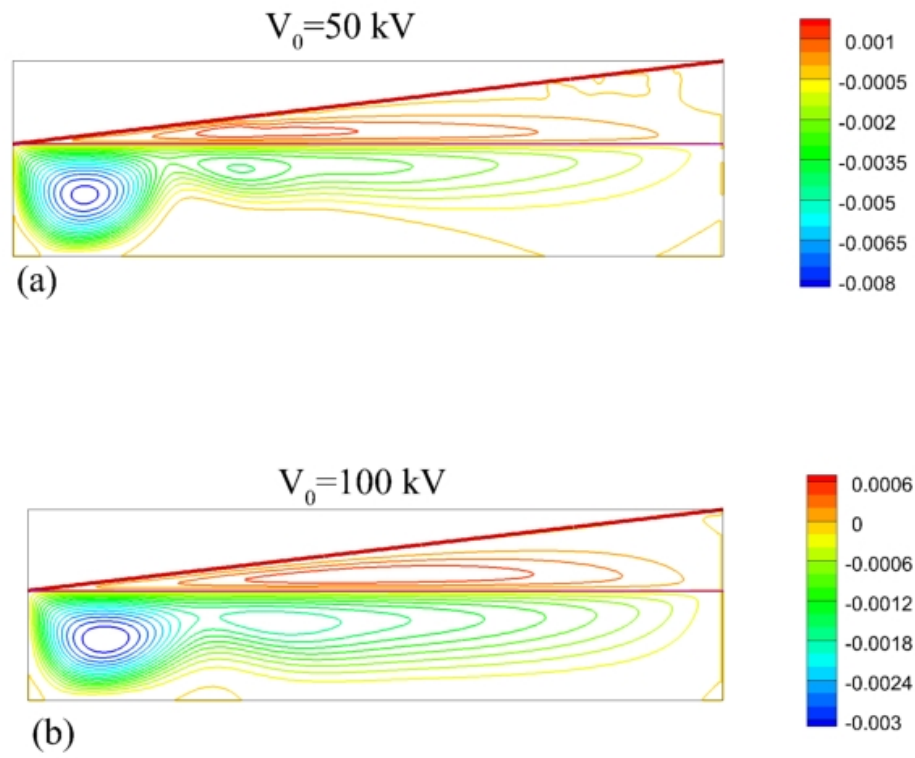


Fig. 4. Change in streamlines with the increase of applied voltage. Along the interface the flow is directed for the right to the left boundary.



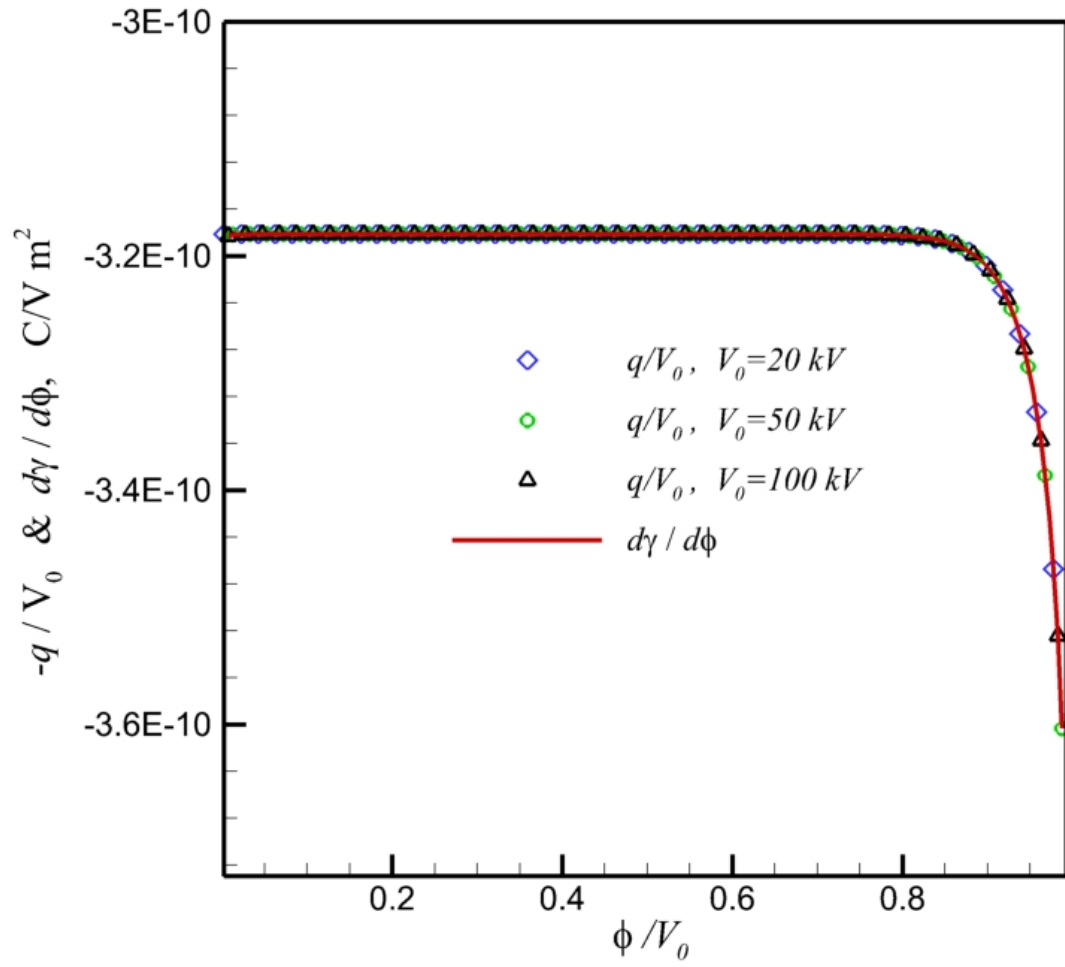


Fig. 5. Illustration of validity of the Lippmann equation: comparison of potential dependence of the surface tension and distribution of the surface charge.